A Stochastically Excited Linear System as a Model for Quasigeostrophic Turbulence: Analytic Results for One- and Two-Layer Fluids

TIMOTHY DELSOLE*

Division of Applied Sciences, Harvard University, Cambridge, Massachusetts

BRIAN F. FARRELL

Department of Earth and Planetary Sciences, Harvard University, Cambridge, Massachusetts

(Manuscript received 26 April 1994, in final form 25 January 1995)

ABSTRACT

The authors explore the hypothesis that nonlinear eddy interactions in quasigeostrophic turbulence can be parameterized as a stochastic excitation plus an augmented dissipation in a statistically stationary equilibrium. The focus is primarily on models sufficiently simple to be solved analytically. In particular, closed form solutions are obtained for the linear response to stochastic excitation of horizontally uniform barotropic and two-layer baroclinic flow. The response of the barotropic model is very simple to understand because the governing equations are mathematically normal. In contrast, the two-layer model is non-normal in the presence of vertical shear and/or vertically asymmetric dissipation and yields rather complicated results. The space–time spectra of the streamfunction and the heat fluxes derived from the two layer model are in qualitative agreement with the corresponding observed quantities at 50°N. The velocity variance predicted from the parameterization is a weaker function of the temperature gradient than indicated by observations. For strong thermal forcing, the parameterized fluxes vary inversely with the difference between a critical temperature gradient and the ambient gradient. This parameterization yields behavior suggestive of baroclinic adjustment but operates by mechanisms fundamentally different from those conventionally associated with instability theory.

1. Introduction

That a flow need not support exponentially unstable normal modes for either transition to or maintenance of turbulence is demonstrated by the existence of turbulence in stable fluid flows (see Lee and Held 1991; Orszag 1971; Davies and White 1928 for examples in two-layer baroclinic flow, Poiseuille flow, and Couette flow, respectively). Nevertheless, particular eddy statistics are frequently consistent with the modal structures derived from the time mean flow; an explanation is needed for why normal mode theory sometimes yields useful results despite clear countercases to its application. We suggest in this work a theoretical framework for understanding the role of linear dynamics in a turbulent, statistically stationary equilibrium by making use of an analysis based on stochastically excited systems.

Suppose the nonlinear equations of motion are written in the form

$$\frac{\partial \phi_i}{\partial t} = \mathbf{W}_i(\phi_1, \phi_2, \phi_3, \cdots, \phi_N) = \mathbf{W}_i(\phi), \quad (1)$$

where ϕ_i is the ith component of an N-dimensional state vector. We decompose the equations into a time-mean component, denoted by a bar, and a deviation therefrom, denoted by a prime quantity. We assume that a statistically stationary state exists. The nonlinear operator can be expanded

$$\mathbf{W}_i(\phi) = \mathbf{W}_i(\bar{\phi}) + \left(\frac{\partial \mathbf{W}_i}{\partial \phi_j}\right)_{\bar{\phi}} \phi_j' + \frac{1}{2}\left(\frac{\partial^2 \mathbf{W}_i}{\partial \phi_j \partial \phi_k}\right)_{\bar{\phi}} \phi_j' \phi_k' + \mathbf{W}_i''', \quad (2)$$

where $\mathbf{W}_i'''$ denotes the third- and higher-order nonlinear terms in perturbation quantities. This last

* Current affiliation: Data Assimilation Office, Laboratory for Atmospheres, NASA Goddard Space Flight Center, Greenbelt, Maryland.

Corresponding author address: Timothy DelSole, Code 910.3, Data Assimilation Office, Laboratory for Atmospheres, NASA Goddard Space Flight Center, Greenbelt, MD 20771.

term vanishes for the Navier–Stokes equations and for the inviscid primitive equations (in Cartesian coordinates) because the advection terms are at most quadratically nonlinear. The two component equations for linear external forcing and dissipation become

$$\text{MEAN} \quad 0 = \mathbf{W}_i(\bar{\phi}) + \frac{1}{2}\left(\frac{\partial^2 \mathbf{W}_i}{\partial\phi_j\partial\phi_k}\right)_{\bar{\phi}} \overline{\phi_j'\phi_k'} \quad (3)$$

$$\text{EDDY} \quad \frac{\partial\phi_i'}{\partial t} = \left(\frac{\partial \mathbf{W}_i}{\partial\phi_j}\right)_{\bar{\phi}} \phi_j' + \frac{1}{2}\left(\frac{\partial^2 \mathbf{W}_i}{\partial\phi_j\partial\phi_k}\right)_{\bar{\phi}} (\phi_j'\phi_k' - \overline{\phi_j'\phi_k'}). \quad (4)$$

Linear forcing and linear dissipation are assumed for convenience and are not necessary assumptions. In atmospheric systems, the term $\mathbf{W}_i(\bar{\phi})$ includes the radiative driving and frictional dissipation acting on the mean flow as well as the Coriolis and mean-flow nonlinear advection components; the other term in (3) includes the forcing due to Reynolds stresses and heat fluxes. The two equations are not independent since the eddy dynamics governed by (4) must yield eddy correlations that balance the mean flow governed by (3).

In this work we are interested in understanding the turbulent regime, which is statistically steady. One approach to solving (4), which cannot yet be rigorously justified, is to introduce a stochastic process to model the second-order nonlinear terms. Such a stochastic model by itself does not yield a closed set of equations since the statistics of the stochastic process depend on the basic state in an unknown way. Nevertheless, this dependence can be approximately inferred from observations in sufficient detail to derive the general characteristics of the statistics of the equilibrated flow. In this sense, the stochastic approach relates the linear dynamics to the climate statistics and therefore offers a theoretical connection between the linear system and the turbulent flow.

The idea of parameterizing the nonlinear fluctuations as a stochastic process has been examined in some detail for the case of homogeneous turbulence (Kraichnan 1959; Leith 1971; Kraichnan 1976). These studies focus on understanding the cascade of energy to different scales but, owing to a lack of ambient shear, cannot explain the maintenance of eddy energy itself. Moreover, these models involve only normal damping operators and therefore lack the richer behavior associated with non-normal systems. These studies do demonstrate, however, that the last term in (4) cannot be replaced by a stochastic process alone. In general, adding a stochastic process to a linear system injects energy into the system. In many systems the last term in (4) acts to redistribute energy among waves and cannot alter the net perturbation energy. This problem can be overcome by adding a dissipative term along with the stochastic excitation to systematically correct the energy budget. Such a refinement is not at all unphysical: nonlinear wave–wave interactions are expected to inject energy into selected waves and to suppress the growth of waves. Accordingly, we assume that in strongly sheared flows a parameterization capturing the essential properties of the nonlinear wave–wave interactions takes the form

$$\frac{1}{2}\left(\frac{\partial^2 \mathbf{W}_i}{\partial\phi_j\partial\phi_k}\right)_{\bar{\phi}} \left(\phi_j'\phi_k' - \overline{\phi_j'\phi_k'}\right) \overset{M}{=} \epsilon_i(\bar{\phi}) + \mathbf{Z}_{ij}(\bar{\phi})\phi_j', \quad (5)$$

where $\epsilon(\bar{\phi})$ is a stochastic process, $\mathbf{Z}(\bar{\phi})$ is the operator embodying the effective linear dissipation, and the symbol $\overset{M}{=}$ is used to stress the fact that strict equality does not apply and that the right-hand side is used for modeling purposes. Thus, the eddy equation (4) is replaced by the parameterized equation

$$\frac{\partial\phi_i'}{\partial t} \overset{M}{=} \left\{\left(\frac{\partial \mathbf{W}_i}{\partial\phi_j}\right)_{\bar{\phi}} + \mathbf{Z}_{ij}(\bar{\phi})\right\}\phi_j' + \{\epsilon_i(\bar{\phi})\}. \quad (6)$$

In general, both the parameterized excitation and dissipation depend on the basic state in a way that cannot yet be determined within the theory itself. We justify the parameterization by demonstrating that its behavior is fairly successful, in the context of simple models, in reproducing the behavior of the observed atmosphere.

It should be noted that even if the basic state is baroclinically unstable, the dynamical system (6) is always stabilized by including the effective dissipation. That this is so follows from two undisputed facts: transient eddies are equilibrated in the present climate and the time-lagged correlations asymptotically decreases with time lag. In physical terms, requiring the mean state to be stable in the stochastic model ensures that the turbulent flow reaches a statistically stationary state. If an unstable dynamical operator is used in the stochastic model, the correlations of meteorological fields would increase with time lag and the system would never achieve steady state.

Farrell and Ioannou (1993a,b, 1994) have recently applied this parameterization to laboratory and geophysical flows and found encouraging results. We extend their work by focusing on analytically solvable models so that the dependence on parameters can be more easily understood. We deal primarily with the quasigeostrophic barotropic and two-layer baroclinic model with horizontally uniform basic states. The excitation is chosen to be of the form

$$\overline{\epsilon(\bar{\phi}, \mathbf{x}, t)\epsilon^H(\bar{\phi}, \mathbf{x}', t')} = \mathbf{Q}\delta(\mathbf{x} - \mathbf{x}')\delta(t - t'), \quad (7)$$

where δ is the Dirac delta function and superscript H denotes the conjugate transpose. If the excitation has some specified correlation pattern, the associated response is found by convolving the excitation with the response due to delta correlated excitation. This allows us to include, for example, the organizing and scale selecting influence of stationary waves by choosing an appropriate excitation. The assumption of white noise is not too restrictive because the wave response is negligible outside a preferred band of frequencies. For lack of justification to do otherwise, we assume the effective dissipation is simple Rayleigh damping.

The effective dissipation can be crudely estimated from observational data using the following general property: time-lagged covariances derived from stochastically excited, linear systems decay with a timescale comparable to the least damped mode. Using essentially this fact in a different stochastic parameterization, Stone et al. (1982) estimated this decorrelation time to be around 2 days from NMC data for three Januarys. The unfiltered, time-lagged correlations of the 300-mb meridional velocity derived from seven winters of ECMWF analyses compiled by Chang (1993) also suggests that this decorrelation is about 2–5 days at 40°N. A similar analysis by Lim and Wallace using high-pass filtered geopotential height (retaining periods less than 7 days) revealed a similar decay timescale for all heights. It should be noted that decorrelation times estimated from low-pass-filtered data are inappropriate for use in the stochastic parameterization because the nonlinear fluctuations are expected to have significant high-frequency components. In this work, we simply assume that the decorrelation time is between 2 and 5 days throughout the extratropical tropopause. This dissipation time represents the combined effect of all damping processes acting on the eddies.

From a spectral perspective, the parameterized excitation can be identified with nonlinear wave–wave interactions. Note that the excitation does not include the energy conversion from mean to eddy since this is captured by the linear operator. Observational analyses by Kung and Tanaka (1983) and Boer and Shepherd (1983) show that the first 10 zonal wavenumbers have individual net transfer rates in the range 0.01–0.1 W m^{-2}. The stochastic excitation also includes eddy forcing by nongeostrophic processes and by external processes such as radiative and latent heating. Peixoto and Oort (1992) estimated from numerical results and residuals based on observational data that radiative and latent heating injects 0.7 W m^{-2} into eddy energy, but nearly all of this forcing is due to latent heating that occurs on scales much smaller than the Rossby radius. Geostrophic adjustment studies imply that only a small fraction of this forcing will couple to the large-scale quasigeostrophic flow, but the efficiency of this coupling is uncertain. Nevertheless, given that the net conversion from mean to all eddies is 1–2 W m^{-2}, a nonlinear exchange rate of 1 W m^{-2} is not unreasonable.

In the next section, we briefly review the analysis of stochastically excited differential equations; the reader familiar with this standard material may skip it. In section 3 we analytically solve the particularly simple case of the barotropic model and find that the ensemble average variance is proportional to the ratio of driving to damping (for fixed wavenumber). Closed form solutions for the two-layer model are obtained in section 4 and examined in detail. We end by summarizing our results.

2. An introduction to the analysis of stochastically forced systems

Techniques for solving differential equations containing a randomly fluctuating term can be found in the texts by Papoulis (1965), Gardiner (1990), and Risken (1989). We briefly review these techniques in this section. Assume that the perturbation equations with the parameterized nonlinear term can be written approximately as a finite matrix equation

$$\frac{d\psi}{dt} = \mathbf{A}\psi + \epsilon(t), \tag{8}$$

where $\mathbf{A}$ is the sum of the linearized dynamical operator and the effective dissipation operator, as in (6), and $\epsilon(t)$ is a vector of stochastic processes with

$$\overline{\epsilon(t)} = 0 \tag{9}$$

$$\overline{\epsilon(t)\epsilon^H(t')} = 2\pi\mathbf{Q}\delta(t - t'). \tag{10}$$

The superscript H denotes the conjugate transpose, and $\mathbf{Q}$ is the forcing covariance matrix. It is a standard result that if $\mathbf{A}$ in (8) has at least one eigenvalue with positive real part, the system is unstable and the response diverges (Noble 1969). Consistency with observation therefore requires assuming that the system is stable when the effective dissipation is included.

With the choice of the transform pair

$$f(t) = \frac{1}{2\pi}\int_{-\infty}^{\infty} f(\omega)e^{-i\omega t}d\omega$$

$$f(\omega) = \int_{-\infty}^{\infty} f(t)e^{+i\omega t}dt, \tag{11}$$

the linear equations (8) have the solution

$$\psi(t) = \frac{1}{2\pi}\int_{-\infty}^{\infty} -(i\omega\mathbf{I} + \mathbf{A})^{-1}\epsilon(\omega)e^{-i\omega t}d\omega. \tag{12}$$

Our notation is that a function of time is written explicitly as a function of time and its Fourier transform is written explicitly as a function of ω. Using (9) and (10), we find that the statistical equilibrium response can be written as

$$\overline{\psi(t)} = 0 \tag{13}$$

$$\mathbf{C}^{ab}_{k,l}(\tau) = \overline{\psi_a(\tau + t)\psi^H_b(t)} = \frac{1}{2\pi}\int_{-\infty}^{\infty} \mathbf{C}^{ab}_{k,l}(\omega)e^{-i\omega\tau}d\omega, \tag{14}$$

where

$$\mathbf{C}_{k,l}(\omega) = (i\omega\mathbf{I} + \mathbf{A})^{-1}\mathbf{Q}^H(-i\omega\mathbf{I} + \mathbf{A}^H)^{-1} \tag{15}$$

and ω is evaluated along the real ω axis. The subscripts k and l refer to the zonal and meridional wavenumbers, respectively, and the superscripts a and b represent the matrix element on the ath row, bth column; the superscripts will be used only when necessary. The only singularities of $\mathbf{C}_{k,l}(\omega)$ in the complex plane are the eigenfrequencies of $\mathbf{A}$, which satisfy

$$\mathrm{Det}[i\omega\mathbf{I} + \mathbf{A}] = 0. \tag{16}$$

When $\mathbf{A}$ is diagonalized by the transformation

$$\mathbf{A} = \mathbf{S}\lambda\mathbf{S}^{-1}, \tag{17}$$

where columns of $\mathbf{S}$ are the eigenvectors of $\mathbf{A}$ and λ is the associated diagonal eigenvalue matrix, the integral (14) can be evaluated using residue calculus:

$$\mathbf{C}^{ab}_{k,l}(\tau) = \overline{\psi_a(\tau + t)\psi^*_b(t)} = -\frac{\mathbf{S}_{aj}\mathbf{S}^{-1}_{jk}\mathbf{Q}_{km}(\mathbf{S}^{-1})^*_{nm}\mathbf{S}^*_{bn}}{\lambda_j + \lambda^*_n}e^{\lambda_j\tau}, \tag{18}$$

where repeated indices imply a summation with respect to that index and $\tau > 0$ is assumed. This can also be written as

$$\mathbf{C}_{k,l}(\tau) = \exp(\mathbf{A}\tau)\mathbf{C}_{k,l}(t = 0). \tag{19}$$

If $\mathbf{A}$ has eigenvalues with positive real part, the correlation will increase without bound for large time lags τ. However, the correlations obtained from atmospheric observations decrease asymptotically with the time lag, indicating that the effective dynamical operator $\mathbf{A}$ must have only negative eigenvalues. This observational fact is the basis for assuming that the effective dissipation operator must stabilize the system.

Note that (18) provides a connection between the covariance matrix and the eigenmodes of the linearized equation. From this covariance matrix it is possible to calculate all eddy fluxes appearing in the mean equations (3). In the following, we examine this covariance matrix in two simple atmospheric models.

3. Response of a barotropic fluid to stochastic forcing

As a first example, we consider the linear response to stochastic excitation of a barotropic zonal flow on a doubly periodic beta plane. The perturbation vorticity equation is

$$\left(\frac{\partial}{\partial t} + U\frac{\partial}{\partial x}\right)\nabla^2\psi + \beta\frac{\partial\psi}{\partial x} = -r\nabla^2\psi + \sum_{k=1}^{\infty}\sum_{l=1}^{\infty}\epsilon_{k,l}(t)e^{ikx+ily}, \tag{20}$$

where U is the constant barotropic velocity, β is the meridional gradient of the Coriolis parameter, r is the frictional damping rate, and only the real part is physical. If the temporal Fourier transform is taken as in (11), and the discrete spatial Fourier transform is taken to be

$$g(x) = \frac{1}{2\pi}\sum_{k=-\infty}^{\infty} g_k e^{ikx} \quad g_k = \int_{-\infty}^{\infty} g(x)e^{-ikx}dx \tag{21}$$

$$h(y) = \frac{1}{2\pi}\sum_{l=-\infty}^{\infty} h_l e^{ily} \quad h_l = \int_{-\infty}^{\infty} h(y)e^{-ily}dy, \tag{22}$$

then the transform of (20) becomes

$$\psi_{k,l}(\omega) = R\epsilon_{k,l}(\omega), \tag{23}$$

where

$$R = \frac{1}{i[(k^2 + l^2)(\omega - \omega_R + ir)]}$$

$$\omega_R \equiv kU - \frac{k\beta}{(k^2 + l^2)}. \tag{24}$$

The function R is referred to as the resolvent associated with the wavenumbers k and l. The ensemble average response is

$$C_{k,l}(\omega) = \frac{q_{k,l}}{[(\omega - \omega_R)^2 + r^2](k^2 + l^2)^2} \tag{25}$$

$$C_{k,l}(\tau) = \frac{q_{k,l}e^{-|\tau|r}}{2r(k^2 + l^2)^2}(\cos(\omega_R\tau) - i\sin(\omega_R|\tau|)), \tag{26}$$

where

$$q_{k,l}\delta(t) = \overline{\epsilon_{k,l}(t)\epsilon^*_{k,l}(t)}. \tag{27}$$

These results can be interpreted in the following straightforward manner. The barotropic fluid possesses a Rossby mode with oscillation frequency ω_R and damping rate r. When the fluid is excited by white noise excitation, the spectrum of the response peaks at ω_R. The magnitude at the peak is controlled by the dissipation parameter, r, and in particular a

resonance for which the response diverges exists for $r = 0$. The factor $(k^2 + l^2)^{-2}$ in the response arises because we have chosen to drive the vorticity equation rather than the momentum equations with white noise. The energy injected by the excitation is ultimately dissipated by friction and the eddies receive energy only from the excitation and give up energy to the dissipation.

Assuming that the excitation is white in space, the variance is found by summing (26) at $\tau = 0$ for all k, l and assuming $q_{k,l} = 1$:

$$\sum_{k=1}^{\infty}\sum_{l=1}^{\infty}\overline{|\psi_{k,l}|^2} = \sum_{k=1}^{\infty}\sum_{l=1}^{\infty}\frac{1}{2r(k^2+l^2)^2}. \quad (28)$$

The total energy is therefore

$$E = \sum_{k=1}^{\infty}\sum_{l=1}^{\infty}\frac{(k^2+l^2)}{2}\overline{|\psi_{k,l}|^2} = \sum_{k=1}^{\infty}\sum_{l=1}^{\infty}\frac{1}{4r(k^2+l^2)}. \quad (29)$$

It is not difficult to show that (28) converges while (29) does not for any finite r. Observational evidence indicates that the magnitude of the net wave–wave conversion rates decay fairly rapidly above zonal wavenumber 10 (Kung and Tanaka 1983). A suitable approximation to $q_{k,l}$ is that of a fixed constant for the 10 gravest wavenumbers and vanishing outside this range. This assumption leads to both a finite energy input rate and a finite response.

Farrell and Ioannou (1993a,b, 1994) have pointed out that a key to understanding systems such as (20) is to recognize that the eigenmodes of the system do not exchange energy either with each other or with the background state. This physical property is expressed mathematically by the fact that the underlying dynamical operator is normal (i.e., commutes with its adjoint) when the variables are transformed into generalized velocities that have the property that the variance expressed in these variables is proportional to the energy. The total variance can be evaluated immediately from (18) in the case of a normal dynamical operator and orthogonal forcing functions with variance q:

$$\mathrm{Trace}(\mathbf{C}_{k,l}) = \sum_{j=1}^{N}\frac{q}{-2\,\mathrm{Re}(\lambda_j)},$$

where we have used the fact that $\mathbf{S}\mathbf{S}^H = \mathbf{I}$ for normal systems.

When a non-normal system is forced, however, the disturbances have the potential to exchange energy with the background flow. Stochastic excitation of non-normal systems can lead to extraction of large amounts of energy from the mean flow, whereas stochastic excitation of a normal system leads to disturbances that do not interact with the mean flow and therefore contain only as much energy as the disturbances accumulate from the excitation. The barotropic flow considered above is normal; a barotropic flow generally becomes non-normal when horizontal shear exists. In the next section we consider stochastic excitation of a two-layer model that becomes non-normal in the presence of vertical shear or asymmetric friction (friction applied unequally to the two layers).

4. Response of a two-layer model to stochastic forcing

We assume a zonal mean flow independent of the meridional direction and bounded by meridional walls at $y = 0$ and $y = L_y$. The linearized two-layer equations with stochastic excitation, Rayleigh friction, and thermal damping are (Holton 1992)

$$\left(\frac{\partial}{\partial t} + U\frac{\partial}{\partial x}\right)\nabla^2\psi + H\frac{\partial\nabla^2\theta}{\partial x} + \beta\frac{\partial\psi}{\partial x} = -r_\psi\nabla^2\psi - r_\theta\nabla^2\theta + \epsilon_\psi \quad (30)$$

$$\left(\frac{\partial}{\partial t} + U\frac{\partial}{\partial x}\right)(\nabla^2\theta - 2\lambda^2\theta) + H\frac{\partial(\nabla^2\psi + 2\lambda^2\psi)}{\partial x} + \beta\frac{\partial\theta}{\partial x} = -r_\psi\nabla^2\theta - r_\theta\nabla^2\psi + 2\lambda^2 r_R\theta + \epsilon_\theta, \quad (31)$$

where

$$\psi = \frac{\psi_{\mathrm{upper}} + \psi_{\mathrm{lower}}}{2} \quad \theta = \frac{\psi_{\mathrm{upper}} - \psi_{\mathrm{lower}}}{2} \quad (32)$$

$$U = \frac{U_{\mathrm{upper}} + U_{\mathrm{lower}}}{2} \quad H = \frac{U_{\mathrm{upper}} - U_{\mathrm{lower}}}{2} \quad (33)$$

$$r_\psi = \frac{r_{\mathrm{upper}} + r_{\mathrm{lower}}}{2} \quad r_\theta = \frac{r_{\mathrm{upper}} - r_{\mathrm{lower}}}{2}, \quad (34)$$

where β is the meridional gradient of the Coriolis parameter; r_ψ and r_θ are the symmetric and antisymmetric damping rates; r_R is the thermal damping rate; $1/\lambda$ is the Rossby radius of deformation such that $\lambda^2 = f_0^2/[\sigma\Delta p^2]$, where f_0 is the Coriolis parameter; Δp is the pressure interval of a single layer; and $\sigma \equiv -RT_0p^{-1}d\ln\theta_0/dp$, for a basic-state potential temperature θ_0 and temperature T_0, and gas constant R. Taking the spatial transform of (30) and (31) using definitions (21) and (22) yields the matrix equation

$$-\mathbf{B}\frac{\partial\phi_{k,l}}{\partial t} = -i\mathbf{D}\phi_{k,l}(t) + \epsilon_{k,l}(t), \quad (35)$$

where

$$\mathbf{B} = \begin{pmatrix} K^2 & 0 \\ 0 & K^2 + 2\lambda^2 \end{pmatrix} \tag{36}$$

$$\mathbf{D} = \begin{pmatrix} -UkK^2 + k\beta + ir_\psi K^2 & -HkK^2 + ir_\theta K^2 \\ -Hk(K^2 - 2\lambda^2) + ir_\theta K^2 & -Uk(K^2 + 2\lambda^2) + k\beta + i(r_\psi K^2 + 2\lambda^2 r_R) \end{pmatrix} \tag{37}$$

$$\phi_{k,l} = \begin{pmatrix} \psi_{k,l} \\ \theta_{k,l} \end{pmatrix} \quad \epsilon_{k,l} = \begin{pmatrix} \epsilon_{\psi k,l} \\ \epsilon_{\theta k,l} \end{pmatrix} \tag{38}$$

$$K^2 = k^2 + l^2. \tag{39}$$

Using (11) to transform the matrix equations to frequency space results in replacing the time derivative by $-i\omega$. The normal modes of the system are the homogeneous solutions of (35) for which the associated eigenfrequencies satisfy

$$\det(\omega\mathbf{B} + \mathbf{D}) = 0. \tag{40}$$

The resulting eigenfrequencies are

$$\omega_\pm = Uk - E - iT \pm F^{1/2}, \tag{41}$$

where

$$E = \left(\frac{k\beta}{K^2}\right)\left(\frac{K^2 + \lambda^2}{K^2 + 2\lambda^2}\right) \tag{42}$$

$$T = r_\psi\left(\frac{K^2 + \lambda^2}{K^2 + 2\lambda^2}\right) + \frac{r_R\lambda^2}{K^2 + 2\lambda^2} \tag{43}$$

$$F = \frac{\lambda^4(ir_\psi - ir_\theta + k\beta/K^2)^2}{(K^2 + 2\lambda^2)^2} + \frac{H^2k^2(K^2 - 2\lambda^2)}{K^2 + 2\lambda^2} - \frac{r_\theta^2K^2}{K^2 + 2\lambda^2} - 2ir_\theta Hk\left(\frac{K^2 - \lambda^2}{K^2 + 2\lambda^2}\right). \tag{44}$$

As usual, stationarity of the statistics is ensured by the stability of the modes. The spectral response to stochastic excitation is therefore

$$\overline{\phi_{k,l}(\omega)\phi_{k,l}^H(\omega')} = \mathbf{S}_{k,l}(\omega)\delta(\omega - \omega') \tag{45}$$

with spectrum

$$\mathbf{S}_{k,l}(\omega) = (\omega\mathbf{B} + \mathbf{D})^{-1}\mathbf{Q}_{k,l}(\omega\mathbf{B}^H + \mathbf{D}^H)^{-1}, \tag{46}$$

where the excitation is defined by

$$\overline{\epsilon(\omega)\epsilon^H(\omega)} = \mathbf{Q}_{k,l} = \begin{pmatrix} q_{k,l}\mathbf{I} \text{ for } k \leq 10 \\ 0 \quad \text{for } k > 10 \end{pmatrix}. \tag{47}$$

Note that condition (47) implies that both the baroclinic and barotropic components of potential vorticity are independently excited at identical magnitudes; the influence of more general excited vertical structures will be examined later. The ensemble covariance matrix for the eddies can be recovered by integration

$$\mathbf{C}_{k,l}(\tau = 0) = \frac{1}{2\pi}\int_{-\infty}^{\infty}\mathbf{S}_{k,l}(\omega)d\omega. \tag{48}$$

We call the trace of $\mathbf{C}_{k,l}(\tau = 0)$ the variance and the trace of $\mathbf{S}_{k,l}(\omega)$ the variance spectrum; these will be denoted by C and $S_{k,l}(\omega)$, respectively.

a. Parameter estimates

Evaluation of the covariance expressions (46) and (48) requires specifying the following 8 parameters: β, L_x, L_y, λ, r_ψ, r_θ, r_R, $q_{k,l}$. The β parameter and the periodic zonal length, L_x, are determined by the choice of latitude. We chose 50°N as our reference latitude because the heat flux maximizes there. Therefore,

$$\beta = \frac{2\Omega}{a}\cos(\phi) \quad L_x = 2\pi a\cos(\phi), \tag{49}$$

where Ω is the earth's rotation rate, a is the radius of the earth, and ϕ is the latitude. The width of the latitude belt should be neither too large, otherwise the β-plane approximation will be violated, nor too small, otherwise the quasigeostrophic approximation will be violated. Lorenz (1979) has noted additional difficulties arising from choosing too small a domain in the context of studying flux parameterizations. We choose the latitudinal width to be 30°, so that

$$L_y \approx 3400 \text{ km} \tag{50}$$

and consider only the five largest meridional wavenumbers that fit inside this dimension; the corresponding wavelengths are approximately 3400 km, 1700 km, 1133 km, 850 km, and 680 km. Because orthogonal waves are excited, the total covariance is simply the sum of the individual covariances.

The parameter r_R is identified with radiative damping, which is generally believed to have a timescale of 10–20 days (Prinn 1977). We fix this parameter at

$$r_R = \frac{1}{20 \text{ days}}. \tag{51}$$

The Rossby radius is typically

$$\lambda \approx 1000 \text{ km} \tag{52}$$

for 50°N.

The parameter $q_{k,l}$ quantifies the stochastic excitation in each layer, and we argued in the introduction that it should be chosen to yield a net injection rate less than 1 W m^{-2} for each of the first 10 zonal wavenumbers. As discussed in section 4e, the injection rate is a function of only $q_{k,l}$, k, l, λ. We choose $q_{k,l}$ to be a constant of such magnitude as to inject 5 W m^{-2} into the combined collection of the first 10 zonal wavenumbers and the first 5 meridional wavenumbers. This choice leads to less than 1 W m^{-2} of excitation for individual zonal wavenumbers as shown in Fig. 1. The influence of the vertical structure of excitation will be discussed in section 4f. The parameters r_ψ and r_θ are identified with the effective dissipation due to nonlinear scrambling and should be chosen to give an overall decorrelation time of 2–5 days. Chang (1993) and Lim and Wallace (1991) present evidence that the decorrelation time is independent of the tropospheric level, suggesting that r_ψ is much larger than r_θ. The ensemble average covariance can be estimated from time averaging a typical realization over a time interval much larger than the timescale of the dynamics. As we will see in the next section, the wave timescale is on the order 2–10 days, so an averaging time as long as a month or a season is needed. This averaging interval is also sufficient to avoid the problems noted by Lorenz (1979). Details of relating covariances derived from the two-layer model to observations are described in the appendix.

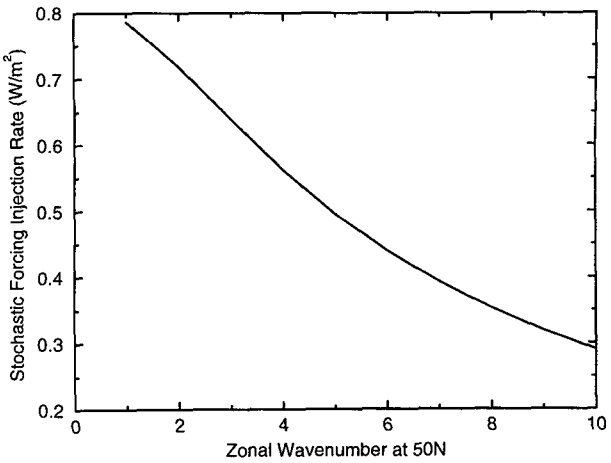

FIG. 1. Energy injection rate due to stochastic excitation as a function of zonal wavenumber for a two-layer model centered 50°N with channel walls separated by 30° lat. Zonal wavenumbers 1–10 and meridional wavenumbers 1–5 are excited in potential vorticity with a combined energy injection rate of 5 W m^{-2}. The Rossby radius is 1000 km. The decay with wavenumber reflects the fact that potential vorticity has been excited white rather than energy.

b. *Variance spectrum*

Since the matrices are 2 × 2, (46) can be easily evaluated:

$$S_{k,l}(\omega) = q_{k,l}\frac{(\omega - Uk)^2(K^4 + (K^2 + 2\lambda^2)^2) + 4k\beta(\omega - Uk)(K^2 + \lambda^2) + \delta}{(K^2(K^2 + 2\lambda^2))^2(\omega - \omega_+)(\omega - \omega_-)(\omega - \omega_+^*)(\omega - \omega_-^*)}, \tag{53}$$

where

$$\delta = 2k^2\beta^2 + 2r_\theta^2K^4 + 2r_\psi^2K^4 + 4r_R^2\lambda^4 + 4\lambda^2r_Rr_\psi K^2 + H^2k^2(K^4 + (K^2 - 2\lambda^2)^2). \tag{54}$$

The variance spectrum is shown in Fig. 2 for parameters chosen to highlight the basic features of the spectrum. The barotropic velocity, U, occurs in (53) only in the Doppler shift form $\omega - kU$. [Note that $\omega_\pm$ contains the term Uk in (41).] Thus, the curve shown in Fig. 2 simply shifts to the left (right) for negative (positive) barotropic velocities. It further follows that when the spectrum is integrated over all frequencies to obtain the variance C, the result is independent of U. The variance spectrum (53) contains the square of the product of the differences between the driving frequency and eigenfrequencies in the denominator, so the frequency of greatest response can plausibly be anticipated to be near the frequency of the least damped mode. The analytic form (53) reveals that $S_{k,l}(\omega)$ decays as $1/\omega^2$ as $\omega \to \infty$ and that $S_{k,l}(\omega)$ will generally have two local maxima located at the real eigenfrequencies of the two modes. These features are indicated in Fig. 2. The total integrated spectrum, which gives the covariance matrix $\mathbf{C}_{k,l}$, is dominated by the area under the peaks of $\mathbf{S}_{k,l}(\omega)$, which are determined to a large degree in this two-layer problem by the damping rate of the eigenmodes. The response to excitation frequencies far away from the eigenmode frequencies are so strongly attenuated that they can be neglected. Thus, the assumption of white noise does not appear to be a serious constraint.

Contours of the variance spectrum as a function of zonal wavenumber and frequency are shown in Fig. 3 for 50°N. Fraedrich and Bottger (1978) present a frequency spectrum of geopotential height obtained from observations at 50°N, which is qualitatively similar to that shown in Fig. 3 derived from the two-layer model.

c. *Total variance*

The area under $S_{k,l}(\omega)$ (divided by 2π) gives the total variance of the response to stochastic excitation. From residue calculus, we find this area to be

$$\overline{\phi_{k,l}^H \phi_{k,l}} = q_{k,l} \frac{T(K^4 + (K^2 + 2\lambda^2)^2)(\mathrm{Re}[F] + T^2 - E^2) + 4\lambda^4 E(2ET - \mathrm{Im}[F]) + T\delta}{4K^4(K^2 + 2\lambda^2)^2(T^2 - \mathrm{Im}[\sqrt{F}]^2)(T^2 + \mathrm{Re}[\sqrt{F}]^2)}. \quad (55)$$

The total variance is independent of the barotropic velocity U, as pointed out previously. In addition, note from (41) that the decay rates of the two eigenmodes are $T + \mathrm{Im}[\sqrt{F}]$ and $T - \mathrm{Im}[\sqrt{F}]$, the product of which appears in the denominator of (55). The stability of the system requires that $T + \mathrm{Im}[\sqrt{F}]$ and $T - \mathrm{Im}[\sqrt{F}]$ both be positive and ensures that (55) is a positive, finite quantity.

A distinctive feature of the variance is most conveniently illustrated using the following nondimensional parameters

$$H^* = \frac{H\lambda^2}{\beta} \quad K^* = \frac{K^2}{\lambda^2} \quad r^* = \frac{r_\psi \lambda^2}{k\beta}. \quad (56)$$

For simplicity, we assume that the dissipation is identical in the two layers and that explicit thermal damping is negligible so that $r_\theta = r_R = 0$. Instability in the inviscid case ($r^* = 0$) requires

$$H^* > \frac{1}{2} \quad K^* < 2. \quad (57)$$

The normalized variance is shown in Fig. 4a as a function of shear and dissipation for the choice $K^* = 1.4$. As expected, the variance increases with increasing shear and decreasing dissipation. Moreover, for weak dissipation, the shear increases sharply at the critical shear for instability near $H^* \approx 1/2$. The waves near $K^* = \sqrt{2}$, it should be noted, tend to have the largest growth rate for fixed H^*, r^*. For waves $K^* > 2$, all waves are stable regardless of the shear, and the variance turns out to be relatively independent of the shear. Remarkably, the variance is also relatively independent of the shear even for waves $K^* < 2$ if the ambient shear is "far" from the corresponding critical shear, as is illustrated in Fig. 4b for the case $K^* = .3$ in which the critical shear is near $H^* = 1.5$. These results indicate the general fact that the variance varies most strongly near the stability boundary. It is remarkable that the variance is virtually independent of shear for waves that have no critical shear or critical shears relatively far from the ambient shear.

The eddy energy is obtained by simply multiplying the variance by K^2 and is shown in Fig. 5 for various choices of effective dissipation. Also plotted are the observed seasonally averaged transient velocity variance based on 8 years of European Centre for Medium-Range Weather Forecasts (ECMWF) analysis compiled by Schubert et al. (1990). The comparison reveals that the magnitude of the observed variance can be modeled by the two-layer model but that the seasonal variations probably require adjusting the effective dissipation (and implicitly the magnitude of excitation). Nevertheless, the observed variations appear to be within the range of dissipation rates inferred from observations. The individual response of the first 9 zonal wavenumbers is shown in Fig. 6 as a function of temperature gradient. The inverse relation of variance to total wavenumber is clearly indicated at vanishing temperature gradient. Although wavenumbers 3 and 4 have critical shears at 28 and 30 K, respectively, and diverge at those values, the variance varies only weakly with temperature gradient far from these gradients.

d. Heat flux

Since $v\theta \approx \overline{\psi_x \theta} = k\,\mathrm{Im}[\psi^* \theta]$, the ensemble average heat transport can be calculated from the off-diagonal elements of the covariance matrix, which in turn can be calculated by residue calculus from (46) and (48). The result is

$$\overline{v'\theta'} = q_{k,l}\lambda^2 k^2 \frac{\beta r_\theta(r_\psi K^2 + r_R\lambda^2) + \mu}{2[K^4(K^2 + 2\lambda^2)^3](T^2 - \mathrm{Im}[\sqrt{F}]^2)(T^2 + \mathrm{Re}[\sqrt{F}]^2)} \quad (58)$$

$$\mu = H(r_\theta^2 K^2(K^2 + \lambda^2) - r_R^2\lambda^2(K^2 - \lambda^2) + r_\psi^2 K^2(K^2 + \lambda^2) - r_R r_\psi[K^4 - 2\lambda^2 K^2 - 2\lambda^4]). \quad (59)$$

The heat flux (58) contains a term inversely proportional to the product of decay rates of the modes, just as does the expression for variance (55). The perturbation variance is maintained at an elevated level primarily by extracting mean available potential energy through downgradient heat transport. Because of this relation, contour plots of heat flux are similar to plots of variance. In the absence of asymmetric friction ($r_\theta = 0$), the direction of the heat flux inferred from (58) has the same sign as the shear H, so the heat flux is downgradient in this case. In the case of vanishing shear ($H = 0$), (58) indicates that the heat flux is pro-

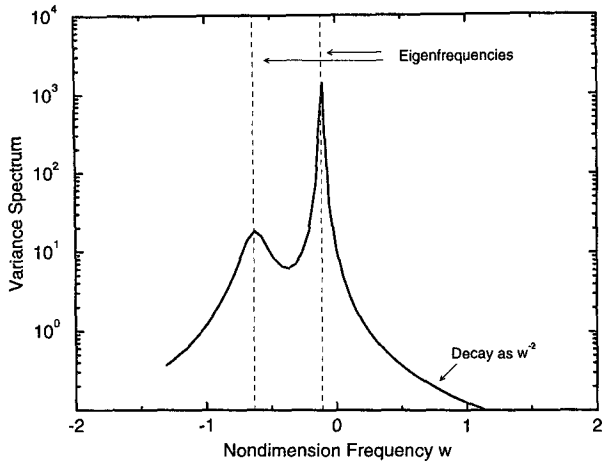

FIG. 2. Frequency spectrum of the variance of the two-layer model response to white noise excitation of a single wavenumber. The spectrum has been nondimensionalized by $(\beta^2\lambda^2 q_{k,l})^{-1}$ and the frequency has been nondimensionalized by $(\lambda/\beta)^{-1}$. The parameters have been chosen to highlight the double peaks and the ω^{-2} decay.

portional to βr_θ. Typically, r_θ is negative since friction acts more strongly on the lower layer than on the upper layer (see 34), so that for small shears the heat flux is negative. Nevertheless, the fact that the stochastically excited two-layer model yields mean upgradient heat and potential vorticity fluxes for certain parameter values suggests that mixing-length arguments cannot be used to understand the stochastically excited system in all parameter regimes.

The heat flux as a function of temperature gradient is shown in Fig. 7. Comparison with the observed values obtained from Schubert et al. (1990) (also shown in Fig. 7) reveals that both the magnitude and seasonal variation of heat flux are fairly well captured by this model with these parameters. The contribution of individual wavenumbers to the total flux is shown in Fig. 8, which reveals that most of the transient eddy heat flux is due to wavenumbers 1–5 with a peak at 3. Although the observed transient eddy flux at this latitude appears to peak at wavenumber 5 (A. Solomon 1993, personal communication based on ECMWF analyses for 10 Januarys at 850 mb), the model does predict a peak flux at small wavenumbers and weak fluxes at large wavenumbers, in agreement with observations.

The divergence of heat flux and eddy energy at the critical gradient is a consequence of choosing a constant effective dissipation, which may not be appropriate for all turbulent regimes. For very strong thermal forcing, the turbulent eddies will become more vigorous (as predicted by the parameterization) and enhance the effective dissipation and thereby shift the critical gradient to higher values. Nevertheless, observations indicate that this effective dissipation is nearly always 2–5 e-folding days in the present regime and this constancy has important implications. For one, the effective critical shear represents a relatively constant upper bound to the mean shear. This follows from taking account of wave–mean flow interactions—when thermal driving acts to increase the temperature gradient, the consequent increase in downgradient fluxes can prevent the gradient from exceeding the critical value. Furthermore, the steepness of the flux-gradient slope implies that enhanced radiative forcing could be balanced through modest changes in temperature gradient, in agreement with observations previously invoked as implying the mechanisms underlying baroclinic adjustment (Stone 1978). Whatever the regime, it would be inconsistent to apply the parameterization developed here to basic states associated with unstable dynamical operators (for instance, the covariances would increase with time lag, in contradiction to all available observations).

Note that the model predicts an order of magnitude increase in heat flux in conjunction with a small increase in eddy energy. The reason the two quantities do not increase at the same rate has already been alluded to above: the waves near $K^* = \sqrt{2}$ are more active baroclinically than other waves and dominate the heat transport for a given excitation while the other waves

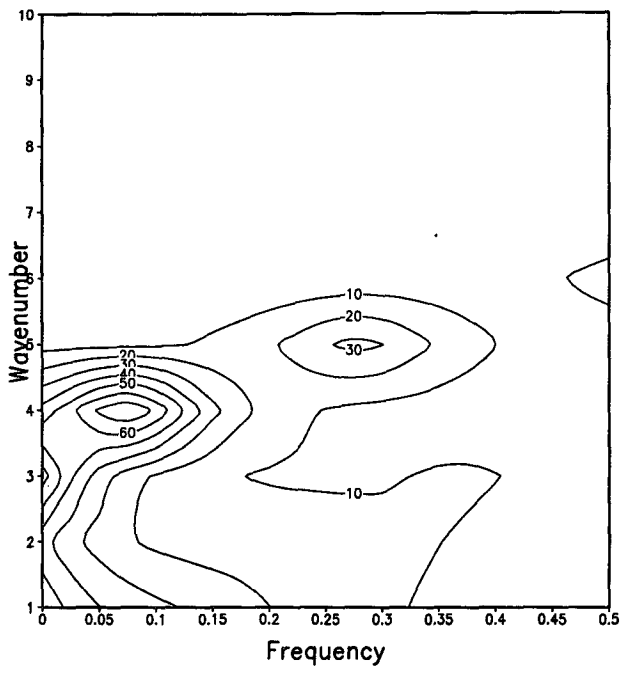

FIG. 3. Contours of the variance spectrum for the stochastically excited two-layer model. The spectrum has been nondimensionalized by $(\beta^2\lambda^2/q_{k,l})^{-1}$, and the frequency is in cycles per day with positive values referring to westward propagation. The horizontal temperature gradient is $T(35N) - T(65N) = 20$ K, the barotropic velocity is $U = 10$ m s^{-1}, the symmetric Rayleigh damping rate is (5 days)$^{-1}$, and the antisymmetric damping rate is (30 days)$^{-1}$.

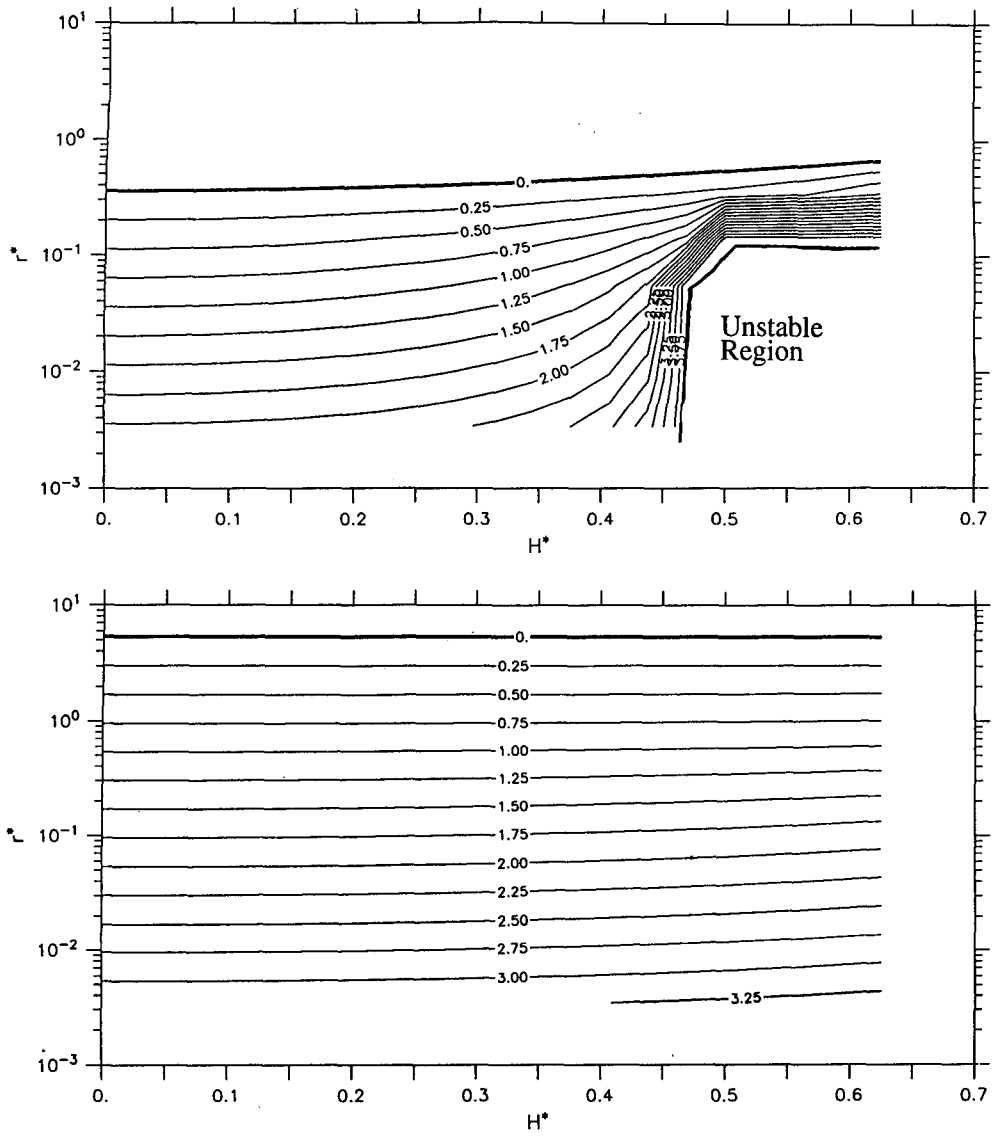

FIG. 4. Log_{10} of the variance of a stochastically excited, horizontally uniform two-layer model as a function of nondimensional dissipation and shear for the case (a) $K^* = 1.4$ and (b) $K^* = 0.3$.

are primarily barotropic and transport relatively little heat. Since the baroclinically active waves make up a small fraction of all waves, their contribution to the total energy at small shears is also a small fraction of the total energy. In contrast, these baroclinically active waves account for virtually all of the stochastically induced heat flux. Moreover, the baroclinically inactive waves tend to grow by injecting energy into eddy available potential energy while leaving the eddy kinetic energy unaltered.

Verifying the consistency of our parameterization using observations is confounded by the fact that the velocity variance in the Northern Hemisphere is significantly affected by stationary forcing by topography. Evidence suggests that this forcing results in low-frequency fluctuations (Blackmon 1976; Blackmon et al. 1977) so that a comparison with band-pass-filtered heat fluxes may allow more precise conclusions regarding the consistency of our parameterization.

e. Energetics

The energy budget equation is obtained by multiplying (30) by ψ, (31) by θ, and integrating over the domain, making use of the boundary conditions. At equilibrium,

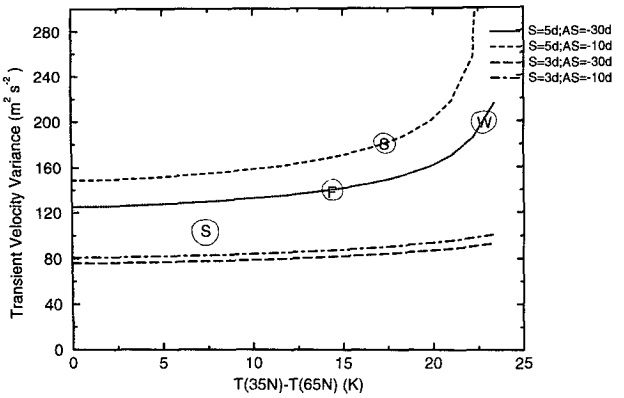

FIG. 5. Vertically averaged velocity variance at 50°N as a function of the vertically averaged temperature difference between 35° and 65°N for the stochastically excited two-layer model (solid line) and the observed seasonal-zonal-vertical average (S = JJA, F = SON, W = DJF, S = MAM; the "S" corresponding to summer is associated with the smallest temperature gradient). The e-folding time for thermal damping is 20 days. The symmetric and asymmetric dissipation are as follows:

dotted $r_\psi = .20\ \text{d}^{-1}$ $r_\theta = -.03\ \text{d}^{-1}$

shortdash $r_\psi = .20\ \text{d}^{-1}$ $r_\theta = -.10\ \text{d}^{-1}$

longdash $r_\psi = .33\ \text{d}^{-1}$ $r_\theta = -.03\ \text{d}^{-1}$

dash–dot $r_\psi = .33\ \text{d}^{-1}$ $r_\theta = -.10\ \text{d}^{-1}$.

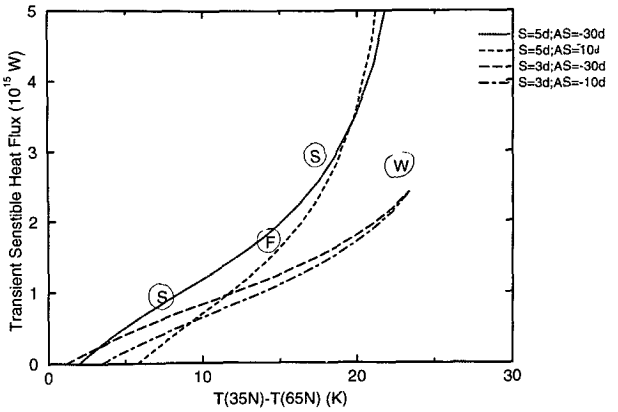

FIG. 7. Net heat flux across 50°N as a function of the vertically averaged temperature difference between 35° and 65°N for the stochastically excited two-layer model (solid line) and the observed seasonal-zonal-vertical average (S = JJA, F = SON, W = DJF, S = MAM; the "S" corresponding to summer is associated with the smallest temperature gradient). The thermal e-folding damping time is 20 days. The symmetric and asymmetric dissipation are as follows:

dotted $r_\psi = .20\ \text{d}^{-1}$ $r_\theta = -.03\ \text{d}^{-1}$

shortdash $r_\psi = .20\ \text{d}^{-1}$ $r_\theta = -.10\ \text{d}^{-1}$

longdash $r_\psi = .33\ \text{d}^{-1}$ $r_\theta = -.03\ \text{d}^{-1}$

dash–dot $r_\psi = .33\ \text{d}^{-1}$ $r_\theta = -.10\ \text{d}^{-1}$.

$$2\lambda^2 H[\psi_x\theta] - [\psi\epsilon_\psi + \theta\epsilon_\theta] - D = 0, \quad (60)$$

where

$$D = r_\psi K^2[\psi^2 + \theta^2] + 2\lambda^2 r_R[\theta^2] + 2K^2 r_\theta[\psi\theta]. \quad (61)$$

The bracket denotes the domain integral. The first term in (60) is called the baroclinic conversion term because it represents the rate at which mean available potential energy is converted to eddy energy. The second term represents the energy injected into the eddy field by the

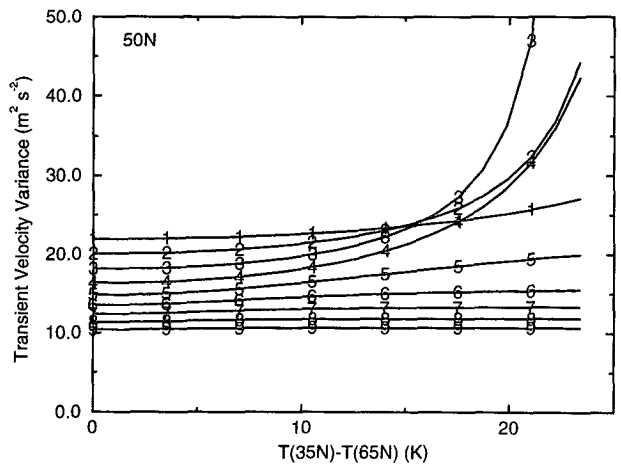

FIG. 6. Vertically averaged velocity variance for zonal wavenumbers 1–9 at 50°N as a function of the vertically averaged temperature difference between 35° and 65°N for the stochastically excited two-layer model. The dissipation is $r_\psi = .20\ \text{d}^{-1}$, $r_\theta = -.03\ \text{d}^{-1}$. The thermal e-folding damping time is 20 days.

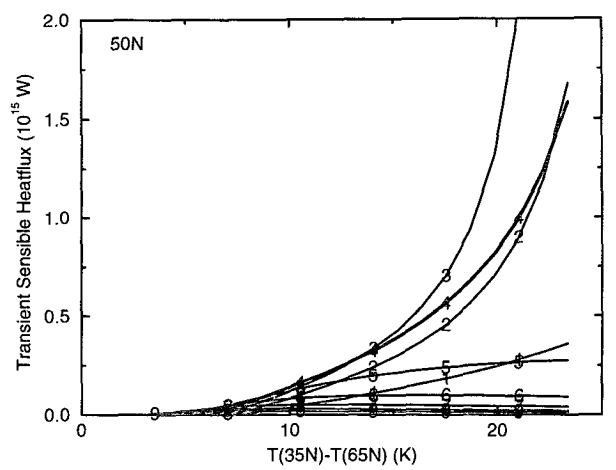

FIG. 8. Heat flux by zonal wavenumbers 1–9 in the stochastically excited two-layer model as a function of the vertically averaged temperature difference between 35° and 65°N. The dissipation parameters are $r_\psi = .20\ \text{d}^{-1}$, $r_\theta = -.03\ \text{d}^{-1}$. The thermal e-folding damping time is 20 days.

stochastic excitation. The last term, D, represents the eddy energy dissipated by surface drag and thermal damping and is always positive. The last term of the dissipation in (61), though related to the dissipation term r_θ, is not always positive as are the other terms. Nevertheless, by rewriting (61) in top/bottom component form rather than baroclinic/barotropic component form, it is straightforward to show that this term together with the first term in (61) always sum to a positive number. The fact that it can be negative is simply an artifact of our decomposing the equations into baroclinic and barotropic forms.

The first two terms in (60) can be calculated directly from the covariance matrix. It is straightforward to use (11), (13), and (35) to show that

$$-[\psi_{k,l}\epsilon_\psi + \theta_{k,l}\epsilon_\theta] = \frac{q_{k,l}}{2}\frac{K^2 + \lambda^2}{K^2(K^2 + 2\lambda^2)}. \quad (62)$$

The input energy decays as $1/K^2$ for large K^2, reflecting our use of an excitation that is white in potential vorticity. Note that the energy injection rate due to the stochastic excitation is independent of the background shear except through this dependence on $q_{k,l}$.

The energy budget (60) is balanced to within roundoff error in our calculations, verifying the consistency of these computations. Since we are concerned here with the general model behavior, we deal with nondimension variables. The variation of the three energy terms when one of k^*, r^*, H^* is allowed to change and the others are held fixed at their standard values is shown in Fig. 9. We have also set $r_\theta = 1/(20$ days) and chosen zonal wavenumber 7 to illustrate an interesting influence of asymmetric friction. At $H^* = 0$, the dissipation balances the excitation. As H^* increases, the disturbances tend to transport heat upgradient and thereby inject energy into the mean flow. Consequently, the rate of frictional dissipation decreases. Note that this implies that the disturbances tend to accelerate a westerly thermal wind for small background temperature gradients. It is clear from (58) that this upgradient transport for sufficiently small shears is due to the combination of the β effect and asymmetric dissipation. For larger shears, the heat transport becomes downgradient and diverges as the critical shear $H^* = .41$ is approached. For small dissipation rates the input energy is balanced in equal proportions by dissipation and conversion from eddy energy to the mean flow. For large dissipation rates the input energy is balanced primarily by dissipation. Note, however, that the baroclinic conversion from mean to eddy reaches a maximum for intermediate dissipation rates. This maximum disappears when the asymmetric friction parameter r_θ is reduced, suggesting that the maximum is due to wave destabilization by asymmetric damping, which is ultimately suppressed by symmetric damping. Finally, the energy balance as a function of zonal wavenumber reveals the $1/K^2$ dependence of the input driving and that this input is primarily balanced by dissipation except near the wavenumbers closest to instability, namely zonal wavenumbers $k^* = 1.5, 1.7$.

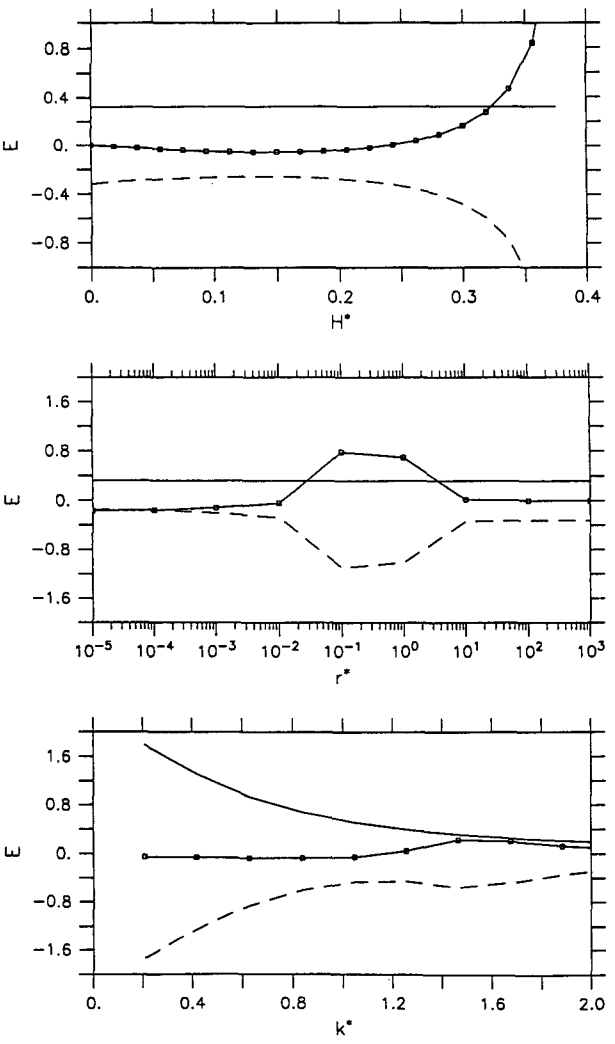

FIG. 9. The nondimensional energy balance between the baroclinic conversion from mean to eddy energy (box), dissipation (dash), and stochastic excitation (solid) as a function of the vertical shear H^* (top), frictional damping rate r^* (middle), and zonal wavenumber k^* (bottom). Only one variable is allowed to vary while the others are fixed at $H^* = .35$, $r^* = .1$, $K^* = 1.4$.

f. Forcing orthogonal functions

The influence of the vertical structure in excitation is most elegantly discussed by using the concept of forcing orthogonal functions (FOFs). These functions provide the orthogonal structures ordered in their contribution to the resulting variance when each is equally excited. These structures represent the counterparts to the empirical orthogonal functions (EOFs) that are or-

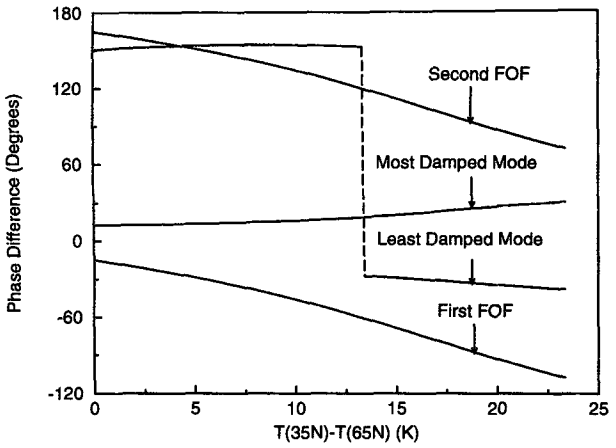

FIG. 10. Phase difference between upper- and lower-layer wave structures of the two normal modes and FOFs of the two-layer model at 50°N as a function of meridional temperature difference. Negative phase differences correspond to disturbances with westward tilts with height. Only the wave with zonal wavenumber 3 and meridional wavenumber 1 is considered since the variance peaks at this wavenumber. The Rossby radius is 1000 km, and the dissipation parameters are $r_\psi = .20\ \mathrm{d}^{-1}$, $r_\theta = -.03\ \mathrm{d}^{-1}$.

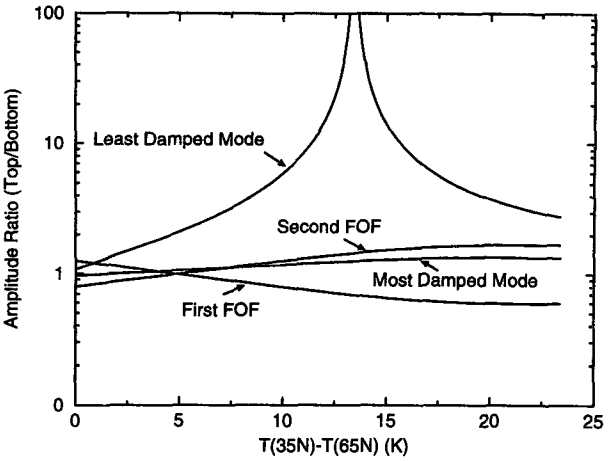

FIG. 11. Amplitude ratio between upper- and lower-layer wave structures of the two normal modes and FOFs of the two-layer model at 50°N as a function of meridional temperature difference. Only the wave with zonal wavenumber 3 and meridional wavenumber 1 is considered since the variance peaks at this wavenumber. The Rossby radius is 1000 km, and the dissipation parameters are $r_\psi = .20\ \mathrm{d}^{-1}$, $r_\theta = -.03\ \mathrm{d}^{-1}$.

thogonal structures ordered in their "explanation" of the observed variance. The appropriate equation for determining the FOFs can be formulated as

$$-\mathbf{B}\frac{d\psi}{dt} = -i\mathbf{D}\psi + e\epsilon(t), \tag{63}$$

where $\epsilon(t)$ is a scalar stochastic process and the vector e has been incorporated to specify the amplitude and relative phase of the vertical structure of the stochastic excitation. Choosing the norm to be simply the variance of the streamfunction, the response can be shown to be

$$\overline{\psi^H(t)\psi(t)} = e^H\mathbf{K}e, \tag{64}$$

where

$$\mathbf{K} = \frac{1}{2\pi}\int_{-\infty}^{\infty}(\omega\mathbf{B}^H + \mathbf{D}^H)^{-1}(\omega\mathbf{B} + \mathbf{D})^{-1}d\omega. \tag{65}$$

The Rayleigh quotient theorem implies that the greatest variance would be achieved when e is the eigenvector of $\mathbf{K}$ corresponding to the largest eigenvalue. The eigenvectors of the hermitian matrix $\mathbf{K}$ are orthogonal and allow ordering the forcing distributions according to their contribution to the variance. These vectors constitute the FOF's.

For the two-layer model, the FOF contains only two unique wave properties of the excitation: the ratio of the amplitudes, r, and relative phase, $\Delta\phi$, between the two layers defined by

$$r = \left|\frac{a_1}{a_2}\right| \quad \Delta\phi = \tan^{-1}\left(\frac{\mathrm{Im}(a_1/a_2)}{\mathrm{Re}(a_1/a_2)}\right), \tag{66}$$

where negative phase corresponds to westward tilts with height and the amplitude factor for each layer is

$$a_1 = e_1 + e_2 \quad a_2 = e_1 - e_2. \tag{67}$$

For large temperature gradients, the phase difference for the two FOF's are identical (Fig. 10) and the first FOF has a slightly larger amplitude in the lower layer

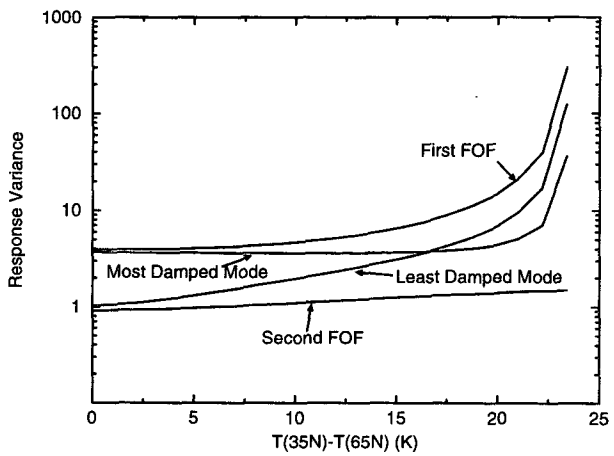

FIG. 12. Streamfunction variance arising from stochastic excitation of potential vorticity with the two FOFs and the two normal modes. The variance has been normalized by the variance obtained by exciting the baroclinic component at vanishing shear. The first FOF yields the largest variance by construction. Only the wave with zonal wavenumber 3 and meridional wavenumber 1 is considered since the variance peaks at this wavenumber. The Rossby radius is 1000 km, and the dissipation parameters are $r_\psi = .20\ \mathrm{d}^{-1}$, $r_\theta = -.03\ \mathrm{d}^{-1}$.

while the second FOF has a slightly larger amplitude in the upper layer (Fig. 11). On the other hand, the first FOF can lead to responses an order of magnitude larger than the second (Fig. 12). These results can be used to infer the change in response due to introducing forcing functions that are correlated in the vertical. In particular, the response will be larger for those functions that project more strongly on the first FOF than on the second.

Consider the case in which the excitation of the barotropic and baroclinic components are statistically independent. The most general forcing function for this case is

$$e = \beta e^{i\delta}\begin{pmatrix} \epsilon_1 \alpha e^{i\gamma} \\ \epsilon_2 \end{pmatrix}, \tag{68}$$

where ϵ_1 and ϵ_2 are real, scalar, independent, unit stochastic excitations and α and β are real. Notice that from (46), (48), the zonal average, statistically steady response depends only on

$$\mathbf{Q} = \overline{ee^H} = \beta^2\begin{pmatrix} \alpha^2 & 0 \\ 0 & 1 \end{pmatrix}. \tag{69}$$

This result implies that the response is independent of the phase difference between the components. Of course, this follows from the fact that the two are excited independently. The velocity variance as a function of α with β adjusted so as to maintain the same net energy injection rate is shown in Fig. 13. The figure illustrates a general fact that we found for a wide range of parameters: forcing the baroclinic component alone typically yields a factor of 2 more variance than forcing the barotropic component alone.

g. *Comments on applying stochastic models as a flux parameterization*

As with other heat flux parameterizations, our result reveals a strong dependence on the mean meridional temperature gradient. Nevertheless, there are distinctive differences. In particular, a parameterization based on Fickian diffusion yields a heat flux proportional to the temperature gradient, whereas ours is inversely proportional to a difference in gradients. This leads to a substantially faster rate of increase in flux with shear than does diffusion. The parameterization based on baroclinic instability and mixing-length theories, as developed by Green (1970) and Held (1974), suggests that for large temperature gradients the heat flux is proportional to the square of the temperature gradient, whereas for small gradients the flux is proportional to the fifth power of the temperature gradient. Both the diffusive parameterization and the parameterizations based on instability theory predict downgradient fluxes for nonzero shears. In contrast, our parameterization suggests a zero flux for positive temperature gradients.

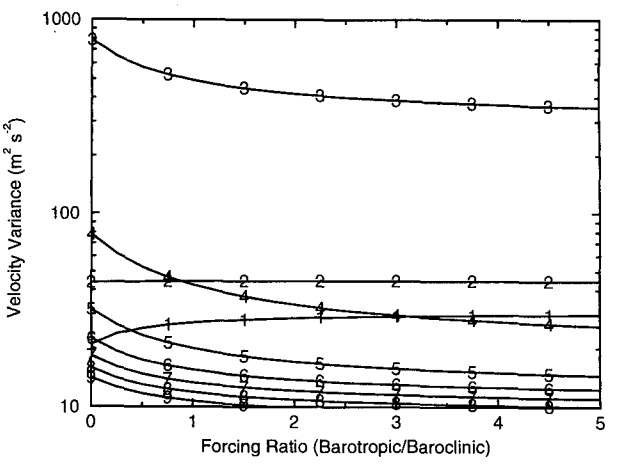

FIG. 13. Velocity variance of zonal wavenumbers 1–10 arising from a stochastically excited two-layer model as a function of the forcing partitioning parameter α; $\alpha = 0$ corresponds to exciting only the baroclinic component, $\alpha = \infty$ corresponds to exciting only the barotropic component. The model is centered at 50°N with a width of 30° lat and meridional wavenumbers 1–5 are excited. The Rossby radius is 1000 km, and the dissipation parameters are $r_\psi = .20\ \mathrm{d}^{-1}$, $r_\theta = -.03\ \mathrm{d}^{-1}$.

As discussed before, this nonzero intercept is due to asymmetric friction in the stochastically excited system.

Consider employing (58) as a parameterization of the atmospheric heat flux as is used in 1D energy balance model (Sellers 1969; Budyko 1969). Extensive study (North 1975; Held and Suarez 1978) indicates that such models obtain equilibrium solutions that are insensitive to the details of the heat flux parameterization. If we consider only the waves $K^* = \sqrt{2}$, which tend to dominate the transport, it is straightforward to show from (58) that

$$\overline{v'T'} = \frac{q_{k,l}H}{4\lambda^4(H_c^2 - H^2)}, \tag{70}$$

where H_c is the critical shear for instability at the given parameters. Assuming that the radiative forcing in midlatitudes is such as to attempt to drive the vertical shear beyond H_c, (70) shows that for small amplitudes of excitation $q_{k,l}$, the heat flux will rise rapidly as H_c is approached and the equilibrated shear will be close to H_c. Indeed, the critical gradient for two-layer instability has been shown to closely approximate the seasonal average temperature gradient (Stone 1978). Thus, for weak stochastic excitation, our parameterization would be expected to yield an equilibrium temperature gradient similar to that resulting from baroclinic adjustment. On the other hand, Held (1978) and Stone (1978) have argued from instability theory that the critical gradient represents a transition from conditions in which deep, efficient waves transport heat to those in

which shallow, inefficient waves transport heat. As Stone (1978) remarks, it is implicit in this explanation that a very rapid transition exists. Our analysis provides an explanation for the existence of a sharp transition, which is otherwise a postulate in linear stability theory—it is due to the inverse flux-shear relation (70) for the equilibrated system and the fact that the effective critical shear of the equilibriated continuous atmosphere happens to be near the critical shear for the two-layer model.

5. Summary and discussion

The response of a linear system associated with horizontally uniform barotropic and two-layer baroclinic models to stochastic excitation was examined in this work. The results have been brought to bear on the hypothesis that the role of nonlinear wave–wave interactions in quasigeostrophic turbulence can be parameterized by stochastic excitation and augmented dissipation. The response of the barotropic model to white noise excitation is very simple to understand: the spectrum of the variance peaks near the Rossby mode frequency and the peak is inversely proportional to the square of the damping rate. The integrated response variance is proportional to the variance of the excitation term and inversely proportional to the damping rate. These results are not fundamentally different from those expected from forcing a damped oscillator. In particular, excited disturbances of a uniform barotropic fluid do not lead to extraction of energy from the background flow, the disturbances receive energy only from the excitation and lose energy only through frictional dissipation. Farrell and Ioannou (1993a,b, 1994) have pointed out that this behavior follows from the normality of the dynamical operator when the governing equations are written in generalized velocity form.

The situation changes considerably in the case of the two-layer model in which the dynamical operator is non-normal when vertical shear exists ($H \neq 0$) and/or asymmetric friction is present ($r_\theta \neq 0$). In this work, closed form expressions for the statistical equilibrium variance and heat flux were obtained [(55) and (58), respectively]. Although the expressions contain a term inversely proportional to the product of the damping rates, the parametric dependence of the response cannot be fully understood without including the remaining terms arising from the non-normality of the underlying system (Farrell and Ioannou 1993b, 1994). For large temperature gradients, the heat flux behaves as

$$\overline{v'T'} \propto \frac{q_{k,l}\Delta T}{\Delta T_c - \Delta T},$$

where ΔT_c is the critical gradient for instability based on the effective dissipation due to nonlinear scrambling. For small positive gradients the flux is proportional to $\beta(r_{\text{upper}} - r_{\text{lower}})$, which suggests that the flux can be upgradient when the dissipation is concentrated in the lower layer. Interestingly, a flux is induced by stochastic excitation even in the absence of a temperature gradient; the analytic solution reveals that this induced flux requires both a β effect and a vertically asymmetric dissipation.

For reasonable parameter choices, comparisons with observations suggest that (58) provides an accurate parameterization of the observed heat flux when the excitation is chosen to inject 5 W m^{-2} into the flow. This corresponds to forcing zonal wavenumbers between 5 and 7 individually at about 0.5 W m^{-2}, which is of the same magnitude of net eddy interaction of those reported by Kung (1988) and Boer and Shepherd (1983) based on observations. For this choice of driving, (55) yields the correct magnitude of the velocity variance but fails to capture the variation of variance with shear. The range of wavenumbers that determine the net heat flux is much smaller than the range of wavenumbers that determine the eddy energy. This point is illustrated in Fig. 14, which shows the baroclinic conversion term $H\overline{v'T'}$, normalized by the energy injection rate due to stochastic excitation, as a function of wavenumber for three values of background shear. Only when the normalized conversion exceeds unity do the eddies extract more energy from the background shear than they accumulate from the stochastic excitation. This level of conversion occurs only for relatively large shears and only for wavenumbers 2–4.

A significant fraction of the changes in intra-annual Northern Hemispheric velocity variance is known to be associated with seasonal changes in stationary wave excitation. These changes are presumably associated with enhanced low-frequency forcing, which cannot be accurately modeled as white noise excitation; our para-

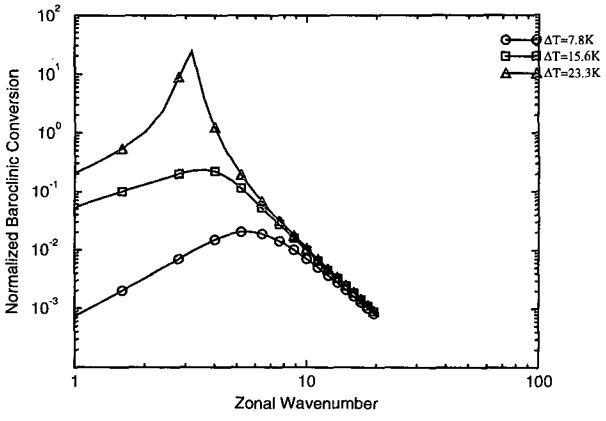

FIG. 14. Baroclinic conversion produced by stochastically excited waves as a function of zonal wavenumber for shears ΔT = 7.8 K (circle), ΔT = 15.6 K (square), and ΔT = 23.3 K (triangle). The conversion is normalized by the injection rate due to stochastic excitation. The Rossby radius is 1000 km, and the dissipation parameters are r_ψ = .20 d^{-1}, r_θ = −.03 d^{-1}.

meterized eddy kinetic energy may be found to be consistent with observations when the large fluctuations associated with stationary waves are properly filtered out.

The present work constitutes a first step in presenting a new physical theory—we have used simple models to gain physical insight into the statistical equilibrium of turbulent fluids. It is a remarkable result that the simplest baroclinic model imaginable can simulate the magnitude and basic behavior of the real atmosphere with approximate estimates of the parameters. A natural consistency question posed by this success is whether the eddy fluxes resulting from stochastic excitation lead to a realistic balance with the mean thermal forcing and therefore to a self-consistent general circulation. This question will be examined in subsequent work.

Acknowledgments. This work is based on a doctoral thesis by T. DelSole. T. DelSole would like to thank Peter Stone and Petros Ioannou for helpful discussions regarding this work, Wayne Higgins for generous help in obtaining the dataset used for the comparisons, and to acknowledge the support afforded by the NASA Global Change Graduate Fellowship. The revisions of this paper were completed while T. DelSole was supported by the U.S. Department of Energy Global Change Distinguished Postdoctoral Fellowship, administered by Oak Ridge Institute for Science and Education, and hosted by the National Aeronautics and Space Administration Goddard Space Flight Center. Brian Farrell was partially funded by the National Science Foundation NSF 9216813 and by the U.S. Department of Energy's (DOE) National Institute for Global Environmental Change (NIGEC) through the NIGEC Northeast Regional Center at Harvard University. (DOE Cooperative Agreement No. DE-FC03-90ER61010.) Financial support does not constitute an endorsement by DOE of the views expressed in this article.

APPENDIX

Correspondence between Model and Observations

In introductory texts such as Holton (1992), it is shown that 1) the streamfunction ψ of the two-layer model is related to geopotential height Φ by

$$\psi = \frac{\Phi}{f_0}, \tag{A1}$$

where f_0 is the Coriolis parameter; 2) the difference in geopotential height is related to the vertical average temperature by the hypsometric equation

$$\Phi_1 - \Phi_2 = R \int_{p_1}^{p_2} T d \ln p, \tag{A2}$$

where R is the gas constant for dry air; and 3) the mass of the vertical column of atmosphere is

$$\frac{\Delta \text{Mass}}{\text{Area}} \approx \frac{\Delta P}{g}. \tag{A3}$$

It is straightforward to use (A1) and (A2) to show that θ, as given by (31) for the two-layer model, is approximately related to the log pressure–averaged temperature by

$$\bar{T} \approx \frac{2 f_0}{R} \theta. \tag{A4}$$

The two-layer heat flux

$$\overline{\frac{\partial \psi}{\partial x} \theta}^x = \frac{1}{2} \overline{\frac{\partial \psi_{\text{upper}}}{\partial x} \theta}^x = \frac{1}{2} \overline{\frac{\partial \psi_{\text{lower}}}{\partial x} \theta}^x \tag{A5}$$

is therefore proportional to the vertically averaged meridional heat flux in the atmosphere. In turn, the zonal average two-layer heat flux is related to the spectral coefficients by

$$\overline{\frac{\partial \psi}{\partial x} \theta}^x = \sum_{k,l} \frac{k}{2} \text{Im}(\psi^*_{k,l} \theta_{k,l}), \tag{A6}$$

where the perturbations are assumed to be harmonic in x and y. Putting this together, we obtain the total heat flux across a latitude,

$$L_x \int_{p_2}^{p_1} c_p \overline{(v'T')}^x \frac{dP}{g} = \frac{2 L_x f_0 c_p (P_1 - P_2)}{Rg} \sum_{k,l} \frac{k}{2} (\psi^*_{k,l} \theta_{k,l}) \tag{A7}$$

and the mean kinetic energy

$$\frac{\frac{1}{2} \iiint ((v')^2 + (u')^2) dx dy dp}{\iiint dx dy dp} = \sum_k \sum_l \left(\frac{k^2 + l^2}{4} \right) (|\psi_{k,l}|^2 + |\theta_{k,l}|^2), \tag{A8}$$

where each layer velocity variance is weighted by half the mass of the atmosphere.

Since the 200-mb level approximates the tropopause level in mid and high latitude, we identify the pressure depth $P_1 - P_2$ with $1000 - 200 = 800$ mb.

It follows from (A4) that the thermal wind relation for the two-layer model is

$$H = \frac{U_{\text{upper}} - U_{\text{lower}}}{2} = -\frac{R}{2 f_0} \frac{\partial \bar{T}^{px}}{\partial y}. \tag{A9}$$

This relation is used to replace H by the corresponding temperature gradients. The temperature gradient can be

simply represented by the temperature difference between two latitude belts.

REFERENCES

Blackmon, M. L., 1976: A climatological spectral study of the 500 mb geopotential height of the Northern Hemisphere. *J. Atmos. Sci.*, **33,** 1606–1623.

——, J. M. Wallace, N-C Lau, and S. L. Mullen, 1977: An observational study of the Northern Hemisphere wintertime circulation. *J. Atmos. Sci.*, **34,** 1040–1053.

Boer, G. J., and T. G. Shepherd, 1983: Large-scale two-dimensional turbulence in the atmosphere. *J. Atmos. Sci.*, **40,** 164–184.

Budyko, M. I., 1969: The effect of solar radiation variations on the climate of the earth. *Tellus,* **21,** 611–619.

Chang, E. K. M., 1993: Downstream development of baroclinic waves as inferred from regression analysis. *J. Atmos. Sci.*, **50,** 2038–2053.

Davies, S. J., and C. M. White, 1928: An experimental study of the flow of water in pipes of rectangular section. *Proc. Roy. Soc. London Ser. A,* **119,** 92–107.

——, and P. J. Ioannou, 1993a: Stochastic forcing of perturbation variance in unbounded shear and deformation flows. *J. Atmos. Sci.*, **50,** 200–211.

——, and ——, 1993b: Stochastic dynamics of baroclinic waves. *J. Atmos. Sci.*, **50,** 4044–4057.

——, and ——, 1994: A theory for the statistical equilibrium energy and heat flux produced by transient baroclinic waves. *J. Atmos. Sci.*, **51,** 2685–2698.

Fraedrich, K., and H. Bottger, 1978: A wavenumber-frequency analysis of the 500 mb geopotential at 50°N. *J. Atmos. Sci.*, **35,** 745–750.

Gardiner, C. W., 1990: *Handbook of Stochastic Methods.* 2d ed. Springer-Verlag, 442 pp.

Green, J. S., 1970: Transfer properties of large-scale eddies and the general circulation of the atmosphere. *Quart. J. Roy. Meteor. Soc.*, **96,** 157–185.

Held, I. M., 1978: The vertical scale of an unstable baroclinic wave and its importance for eddy heat flux parameterizations. *J. Atmos. Sci.*, **35,** 572–576.

——, and M. J. Suarez, 1974: Simple albedo feedback models of the icecaps. *Tellus,* **26,** 613–629.

Holton, J. R., 1992: *An Introduction to Dynamic Meteorology.* Academic Press, 507 pp.

Kraichnan, R. H., 1959: The structure of isotropic turbulence at very high Reynolds numbers. *J. Fluid Mech.*, **5,** 497–543.

——, 1976: Eddy viscosity in two and three dimensions. *J. Atmos. Sci.*, **33,** 1521–1536.

Kung, E. C., 1988: Spectral energetics of the general circulation and time spectra of transient waves during FGGE year. *J. Climate,* **1,** 5–19.

——, and H. Tanaka, 1983: Energetics analysis of the global circulation during the special observation periods of FGGE. *J. Atmos. Sci.*, **40,** 2575–2592.

Lee, S., and I. M. Held, 1991: Subcritical instability and hysteresis in a two-layer model. *J. Atmos. Sci.*, **48,** 1071–1077.

Leith, C. E., 1971: Atmospheric predictability and two-dimensional turbulence. *J. Atmos. Sci.*, **11,** 145–161.

Lim, G. H., and J. M. Wallace, 1991: Structure and evolution of baroclinic waves as inferred from regression analysis. *J. Atmos. Sci.*, **48,** 1718–1732.

Lorenz, E., 1979: Forced and free variations of weather and climate. *J. Atmos. Sci.*, **36,** 1066–1069.

North, G. R., 1975: Theory of energy balance climate models. *J. Atmos. Sci.*, **32,** 2033–2043.

Noble, B., 1969: *Applied Linear Algebra.* Prentice-Hall, 523 pp.

Orszag, S. A., 1971: Accurate solution of the Orr–Sommerfeld stability equation. *J. Fluid Mech.*, **50,** 689–703.

Papoulis, A., 1965: *Probability, Random Variables, and Stochastic Processes.* McGraw-Hill, 583 pp.

Peixoto, J. P., and A. H. Oort, 1992: *Physics of Climate.* American Institute of Physics, 520 pp.

Prinn, R. G., 1977: On the radiative damping of atmospheric waves. *J. Atmos. Sci.*, **34,** 1386–1401.

Risken, H., 1989: *The Fokker-Planck Equation.* Springer-Verlag, 472 pp.

Schubert, S., W. Higgins, C.-K. Park, S. Moorthi, and M. Suarez, 1990: An atlas of ECMWF analyses, parts I and II. NASA Tech. Memo. 100762.

Sellers, W. D., 1969: A global climatic model based on the energy balance of the earth–atmosphere system. *J. Appl. Meteor.*, **8,** 392–400.

Stone, P. H., 1978: Baroclinic adjustment. *J. Atmos. Sci.*, **35,** 561–571.

——, S. J. Ghan, D. Spiegel, and S. Rambaldi, 1982: Short term fluctuations in the eddy heat flux and baroclinic stability of the atmosphere. *J. Atmos. Sci.*, **39,** 1734–1746.

Wallace, J. M., G-H. Lim, and M. L. Blackmon, 1988: Relationship between cyclone tracks, anticyclone tracks and baroclinic waveguides. *J. Atmos. Sci.*, **45,** 439–462.